ANNUAL REPORT OF THE ERWIN L. HAHN INSTITUTE FOR MAGNETIC RESONANCE IMAGING

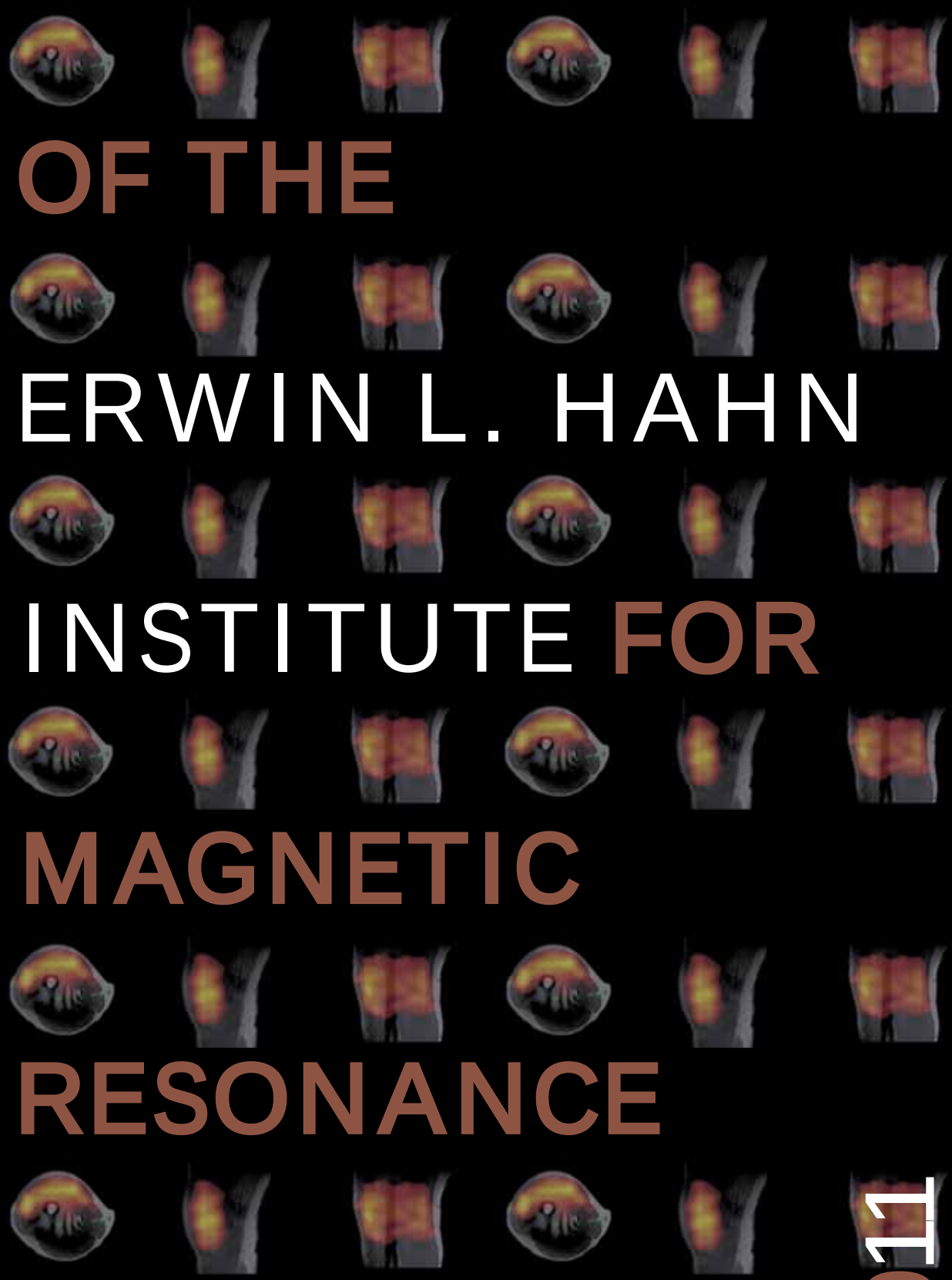

2011

Erwin L. Hahn Institute for Magnetic Resonance Imaging

Arendahls Wiese 199
D-45141 Essen
Germany

t ++49 (0)201-183-6070
f ++49 (0)201-183-6073
w www.hahn-institute.de

Preface

In 2011 the Erwin L. Hahn Institute for Magnetic Resonance Imaging celebrated its fifth anniversary. To mark this event, we decided to expand the normal Erwin L. Hahn Lecture to a symposium with multiple talks and poster presentations. We were very happy to have five internationally well-known experts within different fields of MR research as speakers. The talks highlighted technical and fundamental research aspects as well as several applications of ultra-high-field MR in neuroradiology and cognitive neuroscience. In addition, the experts discussed future benefits and risks related to investing in ultra-high-field MR. Please have a look at the pictures on pages 12 and 13 taken at this exciting event.

On the scientific level, we conducted a wide range of studies and projects within several MR research areas. In 55 projects running at the ELH in 2011, technical challenges, fundamental basic research questions, cognitive neuroscience issues and clinical aspects of ultra-high-field MR were investigated using our 7T scanner. For nine new projects, competitive grants were received in 2011. One important example: Prof. Mark E. Ladd was awarded an „ERC Advanced Investigators Grant“ for his excellent work and received 2.1 million Euros to support his research at the ELH.

The projects of this year and previous work resulted in 22 articles published in internationally acknowledged journals in 2011. In addition, over 75 talks and poster presentations at national and international conferences were held by our team members. One young ELH scientist, Stephan Orzada, received the 3rd place Gorter Award of the German Section of the International Society for Magnetic Resonance in Medicine. And our team was expanded with 13 new members in 2011.

This year, the scientific performance of the ELH was evaluated by a board of internationally well-known experts, and the committee concluded the institute to be in the top 5 of ultra-high-field MR institutes world-wide in terms of scientific productivity.

In this Annual Report the reader will find additional stories of success and some insights into the topics we have been working on at the ELH in 2011 and will hopefully be inspired to contact us for further questions and co-operations.
Matthias Brand

Essen, January 2012.

Structural Connectivity Imaging

Michiel Kleinnijenhuis

Structure Tensor Informed Fiber Tractography by combining gradient echo MRI and diffusion weighted imaging

Structural connectivity research in the human brain in vivo relies heavily on fiber tractography in diffusion-weighted MRI (DWI). The accurate mapping of white matter pathways would gain from images with a higher resolution than the typical ~2 mm isotropic DWI voxel size. Recently, high field gradient echo MRI (GE) has attracted considerable attention for its detailed anatomical contrast even within the white and grey matter. Susceptibility differences between various fiber bundles give a contrast that might provide a useful representation of white matter architecture complementary to that offered by DWI.

Structure Tensor Informed Fiber Tractography (STIFT) is proposed as a method to combine DWI and GE. The GE was acquired at 7T with 0.5 mm isotropic resolution at the Erwin L. Hahn Institute for Magnetic Resonance Imaging. The DWI was acquired at 3T at the Donders Institute (2 mm isotropic, 61 directions). A data-adaptive structure tensor is calculated from the GE image to describe the morphology of fiber bundles. The structure tensor is incorporated in a tractography algorithm to modify the DWI-based tracking direction according to the contrast in the GE image.

By using the structure tensor's first eigenvector (Figure 1; green arrows) to rotate the DWI-based Q-ball vectors (blue arrows) towards the plane parallel to the fiber sheets, the STIFT vectors (red arrows) closely follow the fiber bundles' local orientations, whereas Q-ball vectors fail to capture the details of the morphology. This STIFT adaptation was shown to be beneficial for tractography. From closely spaced seedpoints (0.5 mm) on both sides of the border of the optic radiation (OR) and inferior longitudinal fasciculus (ILF) (Figure 2a), STIFT fiber bundles were clearly separated in white matter (Figure 2c) and terminated in the anatomically correct areas. Fibers seeded in the optic radiation correctly connected primary visual cortex (V1) to the thalamus for STIFT, while Q-ball fibers erroneously connected V1 to anterior temporal and frontal areas. Also the fibers from the ILF seed points were more plausible for STIFT, tracking fibers from extrastriate areas to the temporal and frontal regions. Furthermore, reconstruction of the optic radiation with STIFT showed a larger anterior extent of Meyer's loop compared to the standard tractography alternative. Importantly, by virtue of the GE contrast between the adjacent cingulum and corpus callosum ('kissing' fibers), STIFT adaptation in the multifiber voxels yielded a reduction in crossing-over of streamlines between these tracts, while tracking through the fiber crossings of the centrum semiovale was unaffected [1].

The STIFT method improves the anatomical accuracy of tractography of various fiber tracts, such as the optic radiation and cingulum. Furthermore, it has been demonstrated that STIFT can differentiate between kissing and crossing fiber configurations. Future investigations are required to establish the applicability in more white matter pathways.

[1] Kleinnijenhuis, M., Barth, M., Alexander, D.C., van Cappellen van Walsum, A.-M., and Norris, D.G. (2011). Structure Tensor Informed Fiber Tractography by combining gradient echo MRI and diffusion weighted imaging, NeuroImage (2011), doi:10.1016/j.neuroimage.2011.10.078

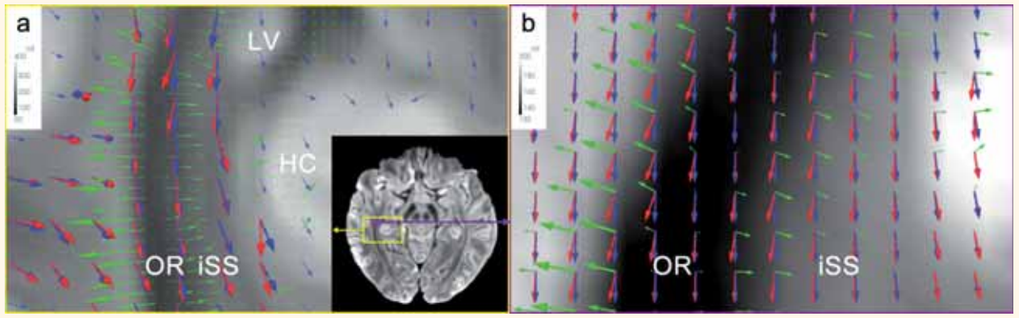

Figure 1: STIFT adaptation. Shown are the structure tensor's 1st eigenvector (PD_{GE}: green arrows), Q-ball 1st peak direction (PD_{DWI}: blue arrows) and STIFT adaptation (PD_{STIFT}: red arrows) on an axial GE slice through the ventral optic radiation (Meyer's loop). a) STIFT adaptation performed at DWI voxel coordinates (Δ=2 mm). PD_{GE} is shown in native GE resolution, but only a random subset of vectors (within the WM mask) is shown as arrows. b) STIFT adaptation performed at GE voxel coordinates (Δ=0.5 mm). PDDWI vectors are linearly interpolated. OR=optic radiation; iSS=internal sagittal stratum; HC=hippocampus; LV=lateral ventricle. Note that the STIFT vectors closely follow the structure of the optic radiation, whereas interpolated Q-ball vectors are not oriented along the tract.

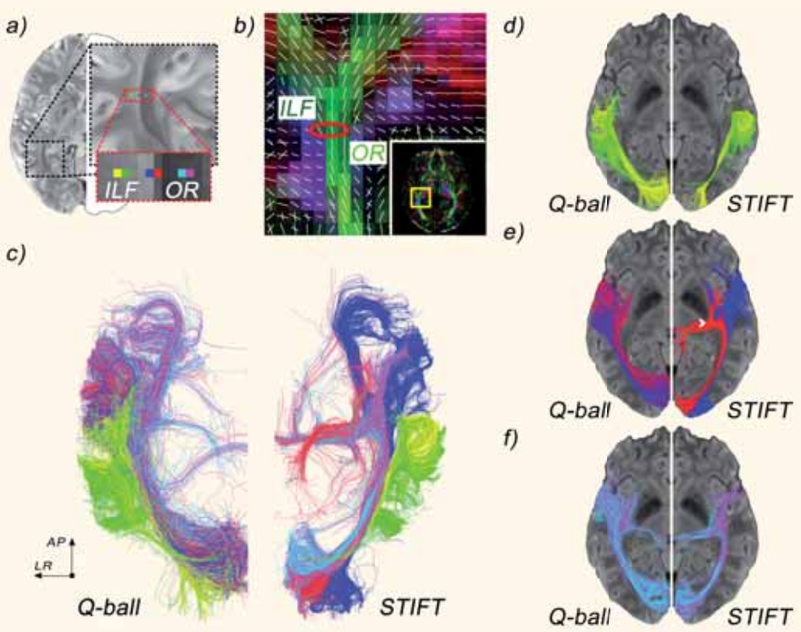

Figure 2: Comparison of standard Q-ball and STIFT in the optic radiation (OR) and inferior longitudinal fasciculus/ occipitofrontal (ILF) fiber tracts. a) set of three seed pairs in the ILF (yellow/ green) the OR (cyan/pink) and one pair on both sides of the border of these tracts (blue/red). b) Q-ball peak directions; red circle indicates the seed location. c) fiber tracts for Q-ball and STIFT: composite image for all six seed points (ventral view). d,e,f) fibers tracts for seeds pairs in the ILF, on the border and in the OR, respectively (ventral view).

Functional Brain Imaging

The sad film paradox – neither sad nor happy but bittersweet! A study on neural correlates of the perception of bittersweet film clips using 7T fMRI

Frank P. Schulte
Nicole C. Krämer

Deliberately watching movies which, at a first glance, make you sad seems to be an awkward behaviour. Yet it is quite common and therefore has been termed the "sad film paradox". Media psychology explains this by suggesting that such movies do not only include sad aspects, but also uplifting, positive messages, and rather elicit "bittersweet" feelings [1]. However, it is still unclear how the brain responds to such bittersweet films. On the basis of the results of recent functional imaging studies which show an involvement of the orbitofrontal cortex (OFC) in complex emotion integration [2], we argue that the OFC should be a key structure in the processing of bittersweet movies. We aimed at contributing to a better understanding of whether or not bittersweet films are more closely related to positive than to negative films, at least on the level of brain responses while watching these films. We also assumed that the limbic system, in particular the amygdala, should be involved in processing positive and negative emotions when watching bittersweet films.

10 neurologically healthy female students took part in the study (mean age 24.80 years). Our participants watched 5 negative, 5 positive and 5 bittersweet movies (for example screenshots see Figure 3) and rated the degree of sadness, funniness, and bittersweetness. The movies were shown again during scanning, and our participants were instructed to relive the emotions they had experienced during the first movie presentation. We acquired functional images on the ELH's 7 Tesla whole-body scanner (Magnetom 7T, Siemens Healthcare, Erlangen, Germany) using a custom-built 8-channel transmit / receive (Tx / Rx) head coil ([3]) and a BOLD contrast sensitive EPI sequence optimized for 7 T functional imaging (also developed at the ELH [4]). General linear models (describing groups of the individually rated top three sad, funny and bittersweet movie clips) were estimated to test our assumptions. Based on prior hypotheses about key brain areas involved we conducted region-of-interest (ROI) analyses in the OFC and the amygdala.
We found that the OFC is consistently activated when bittersweet clips are involved. The left OFC is activated when contrasting bittersweet minus positive clips and also bittersweet minus negative clips, indicating that this might be the region representing the bittersweet component in contrast to the emotional processing elicited by positive or negative clips. Of the reverse contrasts, only the positive minus bittersweet contrast results in a significant albeit more lateral, right-sided activation, indicating that the positive connotation of positive clips is more strongly linked to the right hemisphere than the positive connotation of bittersweet clips. In the contrasts for the simple emotional clips (positive minus negative clips and negative minus positive clips, respectively), the left OFC region is also activated when contrasting positive minus negative clips. The frontal pole is also activated when contrasting bittersweet minus negative movies (Figure 4). Although we found amygdala activation on the single subject level, this activation was interindividually rather different and therefore failed to reach statistical significance on the group analysis level.
Results indicate that the OFC integrates the bitter and the sweet components of bittersweet movies which seem to be more than simple positive or negative emotions. No distinct activations were found within the limbic system, indicating that the three categories of films seem to have induced emotional experiences equally strong and therefore resulting in no significant differential activations in the amygdala. The OFC activation fits to theories which consider it to be the "expanded limbic system" which is involved whenever different emotional aspects have to be integrated in higher cognitive processes, in most cases in strong interaction with the amygdala (e.g., [5],[6],[7]). However, it still has to be analyzed in future studies whether the specificity found here actually is a specificity with regard to emotion quality or whether bittersweet clips share another aspect of specificity concerning their processing.
In this project the chair of General Psychology: Cognition, Prof. Dr. Matthias Brand cooperated with the chair of Social Psychology: Media and Communication at University Duisburg-Essen (Prof. Dr. Nicole Krämer). The two chairs also cooperated at the Erwin L. Hahn Institute for Magentic Resonance Imaging in a project investigating the topic of emotionality in human-robot interaction. The chair of General Psychology: Cognition also examined activity in frontal cortical midbrain structures in a DFG-funded research project on stress and decision making.

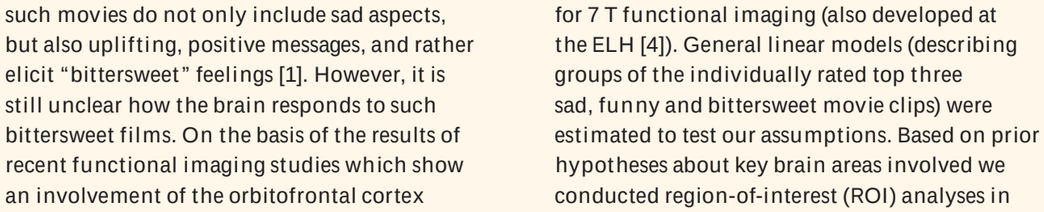

Figure 3: Screenshots of exemplary positive, bittersweet and negative movies

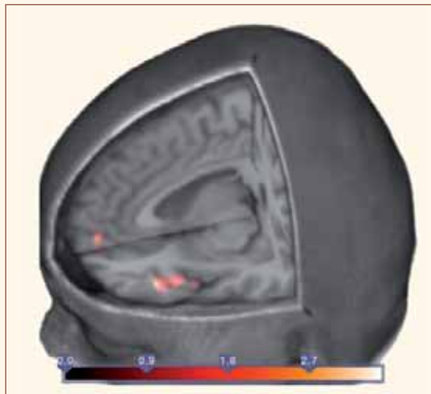

Figure 4: Increased activation was found in OFC and in frontopolar regions of the prefrontal cortex during reception of bittersweet movie clips compared to sad clips (Z-Scores, thresholded at p<0.001 uncorr.).

References:
[1] Oliver M. B. & Woolley J. K.: In K. Döveling et al. (Eds.), Handbook of emotions and mass media; 2010.
[2] Rolls E .T. & Grabenhorst F.: Progress in Neurobiology 2008: 216-244.
[3] Orzada S, et al.; ISMRM 2009: #3010.
[4] Poser BA, et al.; Neuroimage. 2009: 1162-72.
[5] Bechara A, et al.: Cerebral Cortex 2000: 295-307.
[6] Brand M, et al.: Neuropsychologia 2007: 1305-1317.
[7] Stuss DT. & Anderson V.: Brain & Cognition 2004: 69-83.

Whole-Body Imaging

Contrast-enhanced ultra-high-field liver MRI

Lale Umutlu

MR imaging (MRI) of the liver is an accurate imaging modality for the depiction of focal and/or diffuse hepatic disease. Utilization of MRI at 1.5T is considered the clinical standard in most centers. However, initial studies suggest an improved image quality and conspicuity of pathology when higher field strengths such as 3T are used for liver MRI . An increase in the magnetic field strength provides a significant gain in signal-to-noise ratio (SNR), which can be traded off into faster image acquisition and/or improved spatial resolution. Numerous studies have demonstrated the diagnostic potential of high-field MR imaging (> 1.5T) for various organ systems versus 1.5T. The conspicuity of anatomical details can be improved, and the sensitivity and specificity for the depiction of pathological findings can be increased. Despite the anticipated gain in SNR, the transition to higher magnetic field strengths also harbors challenges. Due to tissue susceptibility, chemical shift, and radiofrequency (RF) effects, artifacts can be significantly pronounced at high-field MRI. Moreover, imaging can be impeded by specific absorption rate (SAR) limitations, as the energy deposition increases with the square of the resonance frequency.

Sixteen healthy volunteers (nine male and seven female subjects; average age: 29.5 years, range 26-33 years) were examined in supine position on our 7T whole-body MR system (Magnetom 7T, Siemens Healthcare, Erlangen, Germany). For image acquisition, a custom-built 8-channel RF transmit/receive body coil was used, constructed of two arrays with 4 elements each placed ventrally and dorsally on the upper half of the abdomen (Figure 5). To ameliorate impeding B1 field inhomogeneities, an add-on system for RF shimming was utilized for splitting the excitation signal of the conventional single-channel system into the desired eight channels, and optimized sets of amplitudes and phase shifts provided excitation of specific body regions with enhanced uniformity. Real-time RF supervision was facilitated by logarithmic power meters monitoring forward and reflected power of all eight channels.

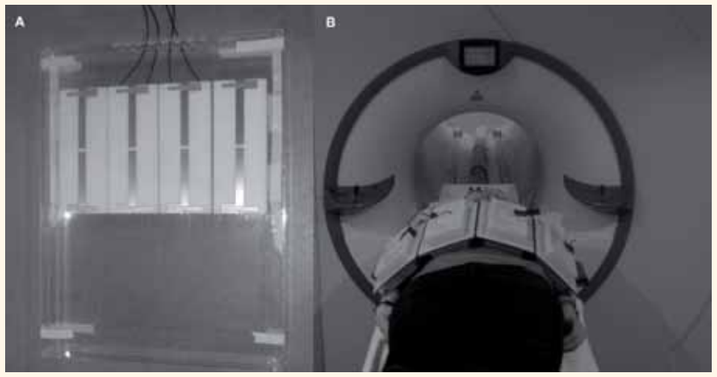

Figure 5: Eight-channel transmit/receive RF array. The healthy subject lies supine on the dorsal array with four stripline meander elements (A). A flexible array also composed of four stripline meander elements is positioned on the ventral upper abdomen (B).

The examination protocol was set up according to a standardized clinical study protocol and adapted to the higher magnetic field strength by modification of imaging parameters. After sequence optimization the following data were acquired: 1) TrueFISP imaging, 2) T2-weighted TSE imaging, 3) T1-weighted in- and opposed-phase imaging, 4) T1-weighted 3D FLASH images obtained pre-contrast and in arterial, portal-venous and venous phases, and 5) a fat-saturated pre- and post-contrast 2D FLASH sequence. Visual evaluation of 1) the delineation of liver vasculature, 2) the overall image quality, and 3) artifact presence and consecutive image impairment was performed by two senior radiologists on a qualitative 3-point scale. SNR of the liver parenchyma was measured for the dynamic 3D FLASH and pre- and post-contrast 2D FLASH sequences.

Fat-saturated 2D FLASH imaging delivered the best mean scores with regard to overall image quality (mean 2.63). In terms of vessel delineation, fat-saturated 2D FLASH (mean 2.65) and in- and opposed-phase imaging (mean 2.75) provided comparably high scores, with post-contrast 2D FLASH revealing particularly improved conspicuity of the peripheral liver vasculature (Figure 6). Quantitative assessment of signal-to-noise ratio in the liver parenchyma in dynamic 3D FLASH MRI showed a continuous increase in SNR from non-enhanced to portal-venous phase imaging, with a slight decrease in contrast-enhancement in the venous phase (Figure 7). Post-contrast 2D FLASH MRI yielded a strong increase in SNR with a statistically significant change versus non-enhanced MRI (p=0.04). While 3D FLASH proved to be the sequence least prone to artifacts (mean 1.17), T2-weighted TSE showed strong impairment due to artifacts (1.97), falling short of diagnostic relevance (Figure 8).

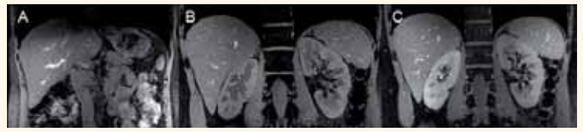

Figure 6: Figure A and B show non-enhanced 2D FLASH MRI, providing high-quality delineation of liver vasculature and excellent overall image quality. Figure B (pre-contrast) and C (post-contrast) demonstrate improvement in liver vessel delineation and homogeneous enhancement of parenchymatous organs of the upper abdomen after contrast media application.

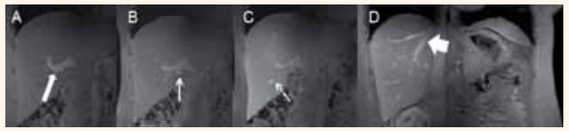

Figure 7: Dynamic 3D FLASH MRI in the (A) non-enhanced, (B) arterial, (C) portal-venous, and (D) venous phases. While the portal veins are well delineated in all phases of dynamic imaging (arrow in Figure A), the liver arteries benefit to some extent from the application of contrast agent (slim arrow in B). Figure C demonstrates improved conspicuity of the peripheral branches of the portal vein (dashed arrow), and D exhibits excellent delineation of contrast-enhanced liver veins.

This pilot study of dedicated contrast-enhanced hepatic imaging at 7T demonstrates the feasibility and challenges of in vivo ultra-high-field liver imaging, providing good overall image quality and very good delineation of non-enhanced vasculature in gradient-echo sequences. T1-weighted 2D FLASH imaging revealed high-quality imaging results, stimulating the idea to perform MR angiography without the need for intravenous gadolinium as a contrast agent. Nevertheless, dynamic imaging showed homogeneous contrast enhancement of liver parenchyma and surrounding abdominal structures as well as an increase in vessel conspicuity. At present, T2-weighted TSE abdominal MRI remains strongly hampered at 7T due to artifacts and SAR restrictions.

In conclusion, this first approach toward dedicated 7T liver MR imaging reveals both opportunities and impediments to ultra-high-field abdominal imaging. Especially non-enhanced angiographic applications appear promising. The initial imaging results demonstrate the successful transformation of the increased SNR into a high spatiotemporal resolution, yielding highly defined non-enhanced and contrast-enhanced anatomical images.

For details of this study see Umutlu L, Bitz AK, Maderwald S, Orzada S, Kinner S, Kraff O, Brote I, Ladd SC, Schroeder T, Forsting M, Antoch G, Ladd ME, Quick HH, Lauenstein TC. Contrast-enhanced ultra-high-field liver MRI: A feasibility trial. Eur J Radiol. 2011 Aug 20. [Epub ahead of print]

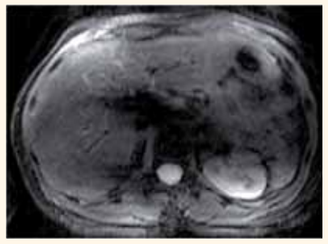

Figure 8: T2-weighted TSE image is strongly impaired at 7T without any relevant diagnostic value.

MRI of X-Nuclei

Imaging of multiple X-nucleus resonances

Tom Scheenen

Nuclei other than protons (X-Nuclei) have a lower resonance frequency and an inherent lower sensitivity in magnetic resonance imaging. Nuclei of interest for studying dynamic changes in cell metabolism in vivo are e.g. ^{13}C and ^{31}P atoms within different molecular structures. Ultra-high magnetic field systems have the potential to bring the information content of metabolites with these nuclei to a clinically acceptable level regarding temporal and spatial resolution. Contrary to the conventional acquisition of a spectral dimension in spectroscopy, we proposed to use the high spectral dispersion of a ultra-high magnetic field to selectively excite only the resonances of interest and image these by a clever choice of imaging parameters.

To accomplish fast imaging of multiple x-nucleus resonances, we introduced a 3D gradient echo (GRE) imaging sequence with a field of view (FOV) in the frequency encoding direction substantially larger than the size of the sample or subject. For excitation of the resonances of interest, we implemented a multi frequency selective Shinnar-Le Roux (SLR) pulse. This SLR pulse excites selected frequency bands with an optimized flip angle and hence excites only the resonances of interest with any desired flip angle. By choosing an appropriate FOV, resolution and readout bandwidth, the frequency separation of metabolite resonances on basis of their chemical shift is enlarged. As a result the selected resonances are imaged next to each other within one image, equivalent to an extreme water-fat shift in conventional proton MRI (Figure 9).

Next to the illustration with a 1-propanol phantom (Figure 9), we verified the method by spatially visualizing the dynamics of energy metabolism during exercise of the upper leg of two healthy volunteers. During exercise, ATP is used to produce energy, and ATP levels are maintained by a rapid exchange in the creatine kinase reaction, catalyzing the formation of ATP from phosphocreatine (PCr), of which the level decreases. After exercise, this reaction is reversed and PCr levels return to normal values. We imaged the levels of ATP and PCr during a simple contraction of the upper leg for two minutes, by selectively exciting the PCr and β-ATP resonance with flip angles in the 3D GRE sequence of 25 and 38 degrees, respectively (TR 500 ms, Figure 10). At a temporal resolution of 2 minutes, a large decrease in PCr was noted localized in the vastus lateralis, while β-ATP remained unchanged (Figure 11b). At a temporal resolution of 20 seconds in the second volunteer the drop in PCr during exercise and the recovery to normal levels could be followed dynamically (Figure 11c).

In conclusion, fast MRI of x-nuclei was realized with a combination of a 3D GRE sequence, frequency selective excitation with an SLR pulse and a separation of different metabolite resonances by exploiting their chemical shift dispersion.

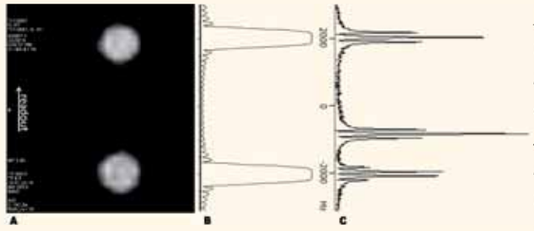

Figure 9: (a) 13C metabolic MR image of a single test tube with 1-propanol. (b) The spectral profile of the Shinnar-Le Roux pulse only excites frequency bands of 500Hz at 2032Hz and -2020Hz, with ramps of 200Hz and flip angles of 90°. (c) The full ^{13}C MR spectrum of the 1-propanol sample. When applying the frequency selective SLR pulse from (b) to the spectrum (c), the triplet at -819Hz is not excited, and the excited resonances at 2032Hz and -2020Hz are well separated. With the following paramaters this resulted in one image of two resonances in the same tube: FOV = 30 × 30 × 80 mm^3, readout bandwidth = 200 Hz/pixel and 3D matrix size = 32 × 32 × 16.

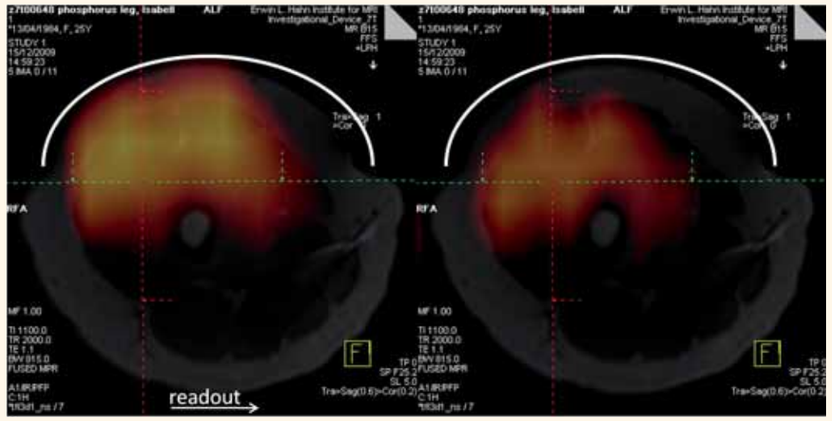

Figure 10: Direct ^{31}P MR image containing a separated map of PCr on the left and β-ATP on the right, overlaid as heatmaps on an axial GRE image of the upper leg of a healthy volunteer. Due to its lower concentration, the signal intensity of β-ATP is lower than that of PCr. For display reasons the 1H MR image of the leg is displayed twice, whereas the ^{31}P MR image is solely one image. The white line illustrates the position of the surface coil. Experimental parameters: FOV 500×500×120mm3, 3D matrix 32×16×16 (interpolated to 32×32×32), readout bandwidth 200Hz/pixel, TR=500ms, TE=5.1ms, 4 averages, 6:50min acquisition time.

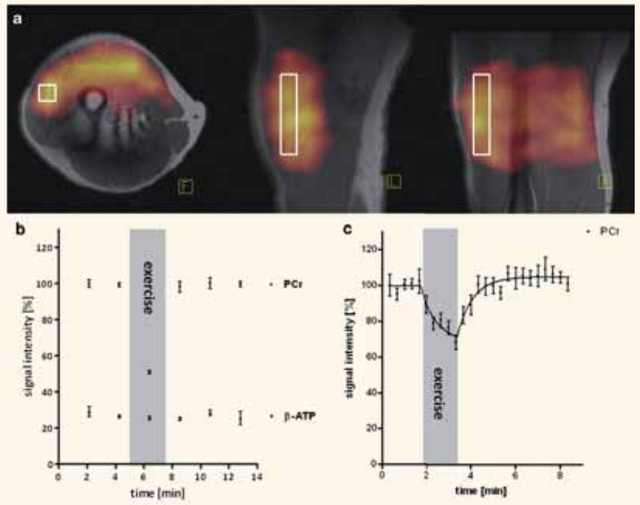

Figure 11: (a) A 3D ^{31}P MR image of PCr fused with 1H anatomical images of the upper leg of a volunteer. The heat map of PCr matched the anatomical shape of the leg within the view of the ^{31}P surface coil. Signals from the white rectangular region of interest inside the vastus lateralis were used to study PCr depletion and recovery during exercise. (b) Signal intensity of PCr and β-ATP before, during and after the contraction of the quadriceps femoris at an intermediate temporal resolution. Note the drop in PCr level to ~50% of rest levels, while β-ATP remains constant. Parameters: matrix size 16×16×16 bandwidth 300Hz/pixel, FOV=500×500×120mm3, TR=500ms, TE=5.1ms, 1 average TA=2:08min. (c) Signal intensity of PCr before, during and after the contraction of the quadriceps femoris of a different volunteer, with a temporal resolution of 20s. The PCr level decreased 30% during the exercise and returned to normal levels in an exponential recovery afterwards. Parameters: FOV of 350×400×120mm3, bandwidth 120Hz/pixel, TR=100ms, TE=7.6ms, TA 20s.

5th Erwin L. Hahn Lecture

The lecture

Lunch in the red dot museum

The location: The red dot museum

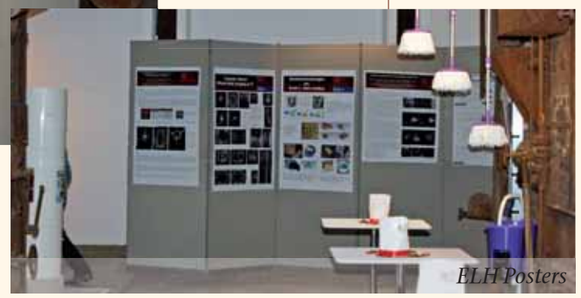

ELH Posters

Thanks to the helpers in the background

The ELH-PIs

Current Grants

Timmann D, Ladd ME, Gizewski ER. Structural and functional magnetic resonance imaging of the cerebellum at 7 Tesla. German Research Foundation; duration: 4 years (August 2007 – September 2011)

Winterhager E. Gruemmer R, Ladd ME. Effects of repeated exposure to strong static magnetic fields from magnetic resonance imagers on the endpoints reproduction and development in an animal model. German Federal Office for Radiation Protection; duration: 3 years (April 2008 – March 2011)

Bayer P, Hoffmann D, Haberhauer G, Ladd ME, Eggert A, Schramm A, Arndt M, Krauss J. ModularProbes: Structure based design of modular MRI probe molecules for the highly sensitive detection of metastases. German Federal Ministry of Education and Research; duration: 3 years (January 2009 – December 2011)

Ladd ME, Rennings A, Solbach K. Competition Science-to-Business PreSeed: MetaCoils – Metamaterial-based high-frequency-coils for 7-Tesla-MRI; duration 3 years (July 2010 – January 2012)

Scheenen T. Exploring the aggressiveness of prostate cancer to enable an individualised treatment approach. European Research Council (ERC Grant); duration 5 years (March 2010 – February 2015)

Brand M, Wolf OT. Stress und Risikoentscheidungen – behaviorale, neuroendokrine und neurale Korrelate der Interaktion von Stress, exekutiven Funktionen und Entscheidungen in Risikosituationen; duration 2 years (October 2010 – September 2012)

Solbach K, Rennings A. Investigation of coil concepts based on flat Electronic Band Gap (EBG) structures for use in magnetic resonance imaging (MRI). German Research Foundation; duration 2 years (January 2011 – December 2012)

Norris D, Tegenthoff M. modulation of inhibitory cortical mechanisms measured using GABA MRS at 7 Tesla. MERCUR; duration 2 years (January 2011 – December 2012)

Timmann D, Ladd ME. Contribution of the human cerebellum to extinction learning and renewal, Project in the Research Unit FOR 1581; German Research Foundation; duration 3 years (January 2011 – December 2013)

Personnel

New in 2011
- Dr. med. Anja Fischer
- Dipl.-Phys. Mirjam Holbach
- Dipl.-Psych. Christian Kaergel
- M.Sc. Tobias Navarro-Schröder
- PD Dr. rer. nat. Bernhard Müller
- Dr. rer. nat. Hasan Nuzha
- Mehmet Ramazanoglu
- B.Sc. Tobias Schöler
- Dr. med. Tobias Schömberg
- Holger Siemann
- Dipl.-Psych. Bettina Staschkiewiez
- Dr. Alejandro Vicente-Graboretsky
- Anna Voß

Left in 2011
- Mark Oehmigen

Publications

Dammann, P., O. Kraff, K.H. Wrede, N. Ozkan, S. Orzada, O.M. Mueller, I.E. Sandalcioglu, U. Sure, E.R. Gizewski, M.E. Ladd, and T. Gasser, *Evaluation of hardware-related geometrical distortion in structural MRI at 7 Tesla for image-guided applications in neurosurgery.* Academic Radiology, 2011. 18(7): p. 910-6.

Diedrichsen, J., S. Maderwald, M. Kuper, M. Thurling, K. Rabe, E.R. Gizewski, M.E. Ladd, and D. Timmann, *Imaging the deep cerebellar nuclei: a probabilistic atlas and normalization procedure.* NeuroImage, 2011. 54(3): p. 1786-94.

Grams, A.E., I. Brote, S. Maderwald, K. Kollia, M.E. Ladd, M. Forsting, and E.R. Gizewski, *Cerebral magnetic resonance spectroscopy at 7 Tesla: standard values and regional differences.* Academic Radiology, 2011. 18(5): p. 584-7.

Grams, A.E., O. Kraff, L. Umutlu, S. Maderwald, P. Dammann, M.E. Ladd, M. Forsting, and E.R. Gizewski, *MRI of the lumbar spine at 7 Tesla in healthy volunteers and a patient with congenital malformations.* Skeletal Radiology, 2011.

Heilmaier, C., J.M. Theysohn, S. Maderwald, O. Kraff, M.E. Ladd, and S.C. Ladd, *A large-scale study on subjective perception of discomfort during 7 and 1.5 T MRI examinations.* Bioelectromagnetics, 2011. 32(8): p. 610-9.

Klomp, D.W.S., T. W.; Arteaga, C. S.; von Asten, J.; Boer, V. O.; Luijten, P. R., *Detection of fully refocused polyamine spines in Prostate cancer at 7 T.* NMR in Biomedicine, 2011.

Koopmans, P.J., M. Barth, S. Orzada, and D.G. Norris, *Multi-echo fMRI of the cortical laminae in humans at 7 T. NeuroImage,* 2011. 56(3): p. 1276-85.

Kraff, O., A.K. Bitz, T. Breyer, S. Kruszona, S. Maderwald, I. Brote, E.R. Gizewski, M.E. Ladd, and H.H. Quick, *A transmit/receive radiofrequency array for imaging the carotid arteries at 7 tesla: coil design and first in vivo results.* Investigative Radiology, 2011. 46(4): p. 246-54.

Kuper, M., A. Dimitrova, M. Thurling, S. Maderwald, J. Roths, H.G. Elles, E.R. Gizewski, M.E. Ladd, J. Diedrichsen, and D. Timmann, *Evidence for a motor and a non-motor domain in the human dentate nucleus--an fMRI study.* NeuroImage, 2011. 54(4): p. 2612-22.

Kuper, M., M. Thurling, R. Stefanescu, S. Maderwald, J. Roths, H.G. Elles, M.E. Ladd, J. Diedrichsen, and D. Timmann, *Evidence for a motor somatotopy in the cerebellar dentate nucleus-an fMRI study in humans.* Human Brain Mapping, 2011.

Meyerspeer, M., T. Scheenen, A.I. Schmid, T. Mandl, E. Unger, and E. Moser, *Semi-LASER localized dynamic (31) P magnetic resonance spectroscopy in exercising muscle at ultra-high magnetic field.* Magnetic Resonance in Medicine, 2011.

Moser, E., F. Stahlberg, M.E. Ladd, and S. Trattnig, *7-T MR - from research to clinical applications?* NMR in Biomedicine, 2011.

Orzada, S., A.K. Bitz, L.C. Schafer, S.C. Ladd, M.E. Ladd, and S. Maderwald, *Open design eight-channel transmit/receive coil for high-resolution and real-time ankle imaging at 7 T.* Medical Physics, 2011. 38(3): p. 1162-7.

Orzada, S., S. Maderwald, B.A. Poser, S. Johst, S. Kannengiesser, M.E. Ladd, and A.K. Bitz, *Time-interleaved acquisition of modes: An analysis of SAR and image contrast implications.* Magnetic Resonance in Medicine, 2011.

Poser, B.A., E. van Mierlo, and D.G. Norris, *Exploring the post-stimulus undershoot with spin-echo fMRI: implications for models of neurovascular response.* Human Brain Mapping, 2011. 32(1): p. 141-53.

Theysohn, J.M., O. Kraff, S. Maderwald, M. Barth, S.C. Ladd, M. Forsting, M.E. Ladd, and E.R. Gizewski, *7 tesla MRI of microbleeds and white matter lesions as seen in vascular dementia.* Journal of magnetic resonance imaging : JMRI, 2011. 33(4): p. 782-91.

Thurling, M., M. Kuper, R. Stefanescu, S. Maderwald, E.R. Gizewski, M.E. Ladd, and D. Timmann, *Activation of the dentate nucleus in a verb generation task: A 7T MRI study.* NeuroImage, 2011. 57(3): p. 1184-91.

Umutlu, L., A.K. Bitz, S. Maderwald, S. Orzada, S. Kinner, O. Kraff, I. Brote, S.C. Ladd, T. Schroeder, M. Forsting, G. Antoch, M.E. Ladd, H.H. Quick, and T.C. Lauenstein, Contrast-enhanced ultra-high-field liver MRI: A feasibility trial. European Journal of Radiology, 2011.

Umutlu, L., O. Kraff, S. Orzada, A. Fischer, S. Kinner, S. Maderwald, G. Antoch, H.H. Quick, M. Forsting, M.E. Ladd, and T.C. Lauenstein, *Dynamic contrast-enhanced renal MRI at 7 Tesla: preliminary results.* Investigative Radiology, 2011. 46(7): p. 425-33.

Umutlu, L., S. Orzada, S. Kinner, S. Maderwald, I. Brote, A.K. Bitz, O. Kraff, S.C. Ladd, G. Antoch, M.E. Ladd, H.H. Quick, and T.C. Lauenstein, *Renal imaging at 7 Tesla: preliminary results.* European Radiology, 2011. 21(4): p. 841-9.

Wrede, K.H., S. Johst, P. Dammann, L. Umutlu, M.U. Schlamann, I.E. Sandalcioglu, U. Sure, M.E. Ladd, and S. Maderwald, *Caudal Image Contrast Inversion in MPRAGE at 7 Tesla Problem and Solution.* Academic Radiology, 2011.

Erwin L. Hahn Institute for Magnetic Resonance Imaging

Arendahls Wiese 199
D-45141 Essen
Germany

t ++49 (0)201-183-6070
f ++49 (0)201-183-6073
w www.hahn-institute.de

Graphic design
AMP Studio, Duisburg

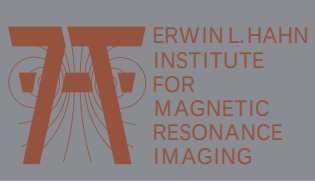

PARTICIPATING INSTITUTIONS

FAKULTÄT FÜR
INGENIEURWISSENSCHAFTEN